Real-time Control Strategy to Maximize Hybrid Electric Vehicle Powertrain Efficiency

Wassif Shabbir*, Simos A. Evangelou

Imperial College London, Department of Electrical and Electronic Engineering, Exhibition Road, London, United Kingdom

Abstract

The proposed supervisory control system (SCS) uses a control map to maximize the powertrain efficiency of a hybrid electric vehicle (HEV) in real-time. The paper presents the methodology and structure of the control, including a novel, comprehensive and unified expression for the overall powertrain efficiency that considers the engine-generator set and the battery in depth as well as the power electronics. A control map is then produced with instructions for the optimal power share between the engine branch and battery branch of the vehicle such that the powertrain efficiency is maximized. This map is computed off-line and can thereafter be operated in real-time at very low computational cost. A charge sustaining factor is also developed and introduced to ensure the SCS operates the vehicle within desired SOC bounds. This SCS is then tested and benchmarked against two conventional control strategies in a high-fidelity vehicle model, representing a series HEV. Extensive simulation results are presented for repeated cycles of a diverse range of standard driving cycles, showing significant improvements in fuel economy (up to 20%) and less aggressive use of the battery.

Keywords: supervisory control, energy management, hybrid electric vehicle, energy efficiency, off-line control

1. Introduction

Over the past decade there has been an increasing awareness of climate change and growing concerns regarding air pollution and the finite supply of fossil fuels. As a result, the whole automotive sector has seen the start of a historical transition towards the electrification of vehicle fleets. This effort has seen growing collaboration and understanding between manufacturers, regulators and researchers to deliver vehicle technologies that are not only environment-friendly but also commercially viable. This transition is therefore expected to depend significantly on the hybrid electric vehicle (HEV), which is seen by some as a stepping stone while others consider it a solution in its own right [1, 2]. It is predicted that by 2020 approximately 18% of new vehicles sold in Europe, and 7% in the US, will be HEVs (while the estimates are 8% and 2% respectively for pure electric vehicles) [3]. It is therefore of significant interest to study how improvements in HEV performance can be made.

Of particular interest is the energy management problem, which involves determining the optimal power allocation between multiple sources in the powertrain. The supervisory control system (SCS) of the vehicle is responsible for addressing this problem with respect to vehicle constraints. The topic has been studied for the past decade and a vast range of SCSs have been proposed in the literature, ranging from rule-based to optimization-based solutions [4, 5, 6, 7, 8, 9]. However, most SCSs of the latter nature involve significant amount of computation and therefore they are not implementable in real-time. Nevertheless, these can serve as important benchmarks to identify a globally optimal solution. Past work has generally applied dynamic programming [10, 11] in this pursuit but more recently convex optimization [12, 13, 14] has emerged as a potent option.

*Corresponding Author

Email addresses: wassif.shabbir07@imperial.ac.uk (Wassif Shabbir), s.evangelou@imperial.ac.uk (Simos A. Evangelou)

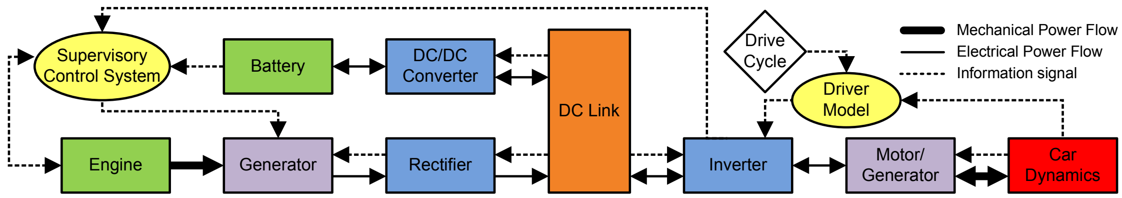

Figure 1: Overview of the architecture of the modelled series HEV.

Various types of equivalent consumption minimization strategies (ECMS) have been pursued [15, 16] for all types of HEVs, as they are computationally feasible in real-time and have been shown to achieve good fuel economy. However, the success of the ECMS is quite sensitive to the equivalence factor between fuel and battery charge that depends on driving cycle and other changing factors. An alternative approach to minimizing equivalent fuel consumption is to maximize the powertrain efficiency. This has the advantage of not only being more intuitive but also less sensitive to tuning, as the component efficiencies are often readily available unlike equivalence factors. Also, this method is more transparent in the sense that it can be understood where the various losses are occurring in the powertrain. Furthermore, this control method does not rely on future driving information but only on the instantaneous power demanded for the vehicle to follow any given speed profile. Therefore, it can be implemented in real-time at low computational cost.

Past work that has taken the approach of considering the powertrain efficiency has often focused on the optimization of the internal combustion engine (ICE) or the engine-generator set, as a vast majority of the powertrain losses occurs there. Consequently, this often results in the battery dynamics and losses being considered very crudely, if not neglected. Instead the battery is only considered when applying constraints on the control, typically to ensure the SOC remains between a defined upper and lower bound. Some work investigates the overall powertrain efficiency but uses it to derive heuristic control rules rather than an efficiency-maximizing objective function [17, 18, 19]. Other work studies the powertrain efficiency in depth to inform the control algorithm (without specifically optimizing efficiency) and then evaluates simulation results rigorously [20, 21]. The proposed work takes a holistic approach and investigates the efficiency of the whole powertrain in depth before producing a control map such that the total efficiency is continuously locally maximized during driving (subject to SOC constraints). The implementation of SCSs using control maps has been done in the past as well [22]. These maps are easy to implement and can be read during driving in real-time with very limited processing requirements. Also, as the maps are precomputed off-line, there is practically no time-constraint on the optimization algorithm to maximize the efficiency.

The control strategy proposed in this paper is an evolution of the algorithm presented in [23, 24]. The main advances involve improvements in the methodology for determining the powertrain efficiency and condensing of the algorithm into a simpler form without loss of performance. Although the method and structure of the proposed control strategy is applicable to HEVs of any architecture, it has been implemented for a series HEV in this work, using the dynamical vehicle model described in [25]. This high-fidelity physics-based model allows complex transient behavior throughout the powertrain, unlike most models that are based on steady-state operation, and thus provides validity to the obtained results. However, due to the complexity of the vehicle model, it hasn't been feasible to compute a global optimal control solution for benchmarking purposes. Instead, the proposed SCS has been benchmarked against two conventional series HEV control strategies: the Thermostat Control Strategy (TCS) and the Power Follower Control Strategy (PFCS). These are widely used as benchmarks in literature for series HEVs.

In the next section the vehicle model is introduced and Section 3 analyzes the powertrain to determine the efficiencies of the energy sources. This analysis forms the foundation for the SCSs discussed in Section 4. Results are presented in Section 5 where the performance in terms of power profiles, SOC and fuel economy are discussed. Finally conclusions are given in Section 6.

Nomenclature

η_{CS}	charge sustaining objective function
η_{dcdc}	DC-DC converter efficiency
η_{ICE}	ICE efficiency
η_{PS}	PS efficiency
η_{rec}	rectifier efficiency
η_{re}	SS replenishing efficiency
η_{SS}	SS efficiency
η_{tot}	combined efficiency of PS and SS
$\omega_{ICE,opt}$	optimal ICE speed for given load
ω_{ICE}	ICE speed
I_{bat}	battery current
k	charge sustaining factor
M_{eq}	normalized equivalent fuel consumption
m_{eq}	equivalent fuel consumption
m_f	mass of fuel consumed by ICE
P_{bat}	battery power
P_{ch}	scaling factor for PFCS
P_{PL}	PL power
$P_{PS,opt}$	PS power at its optimal operating point
P_{PS}	PS power
P_{SS}	SS power
Q	consumed battery charge
Q_{HV}	lower heating value of diesel
s_c	charging equivalence factor
s_d	discharging equivalence factor
SOC	state-of-charge
SOC_L	lower threshold of SOC
SOC_U	upper threshold of SOC
T_{ICE}	ICE torque
u	power share factor
u_{opt}	optimal power share factor
v	correction factor for SS efficiency
$V_{bat,OC}$	battery open circuit voltage
V_{bat}	battery voltage
V_{dc}	DC bus voltage
η^*_{SS}	SS discharging efficiency
ECMS	Equivalent Consumption Minimization Strategy
EMCSM	Efficiency Maximizing and Charge Sustaining Map
EMM	Efficiency Maximizing Map
EUDC	Extra-Urban Driving Cycle
EZ	exponential zone
FTP-75	Federal Test Procedure 75
HEV	hybrid electric vehicle
ICE	internal combustion engine
NYCC	New York City Cycle
PFCS	Power Follower Control Strategy
PL	Propulsion Load (inverter, PMSM and vehicle load)
PMSG	permanent magnet synchronous generator
PMSM	permanent magnet synchronous motor
PS	Primary Source (ICE, PMSG and rectifier)
SCS	supervisory control system
SS	Secondary Source (battery and DC-DC converter)
TCS	Thermostat Control Strategy

2. Vehicle Model

The SCSs presented in this work are designed and tested in the dynamic vehicle model described in [25]. The model consists of a series hybrid powertrain arrangement as shown in Fig. 1, and its parameter set is representative of general-purpose passenger cars. This dynamic model is capable of realistic transient response in the frequency range appropriate for standard driving. The powertrain of the vehicle includes the motor-set which is an inverter driven Permanent Magnet Synchronous Motor (PMSM), mechanically connected to the wheels of the car via a continuously variable transmission. The motor-set driving the car is the Propulsion

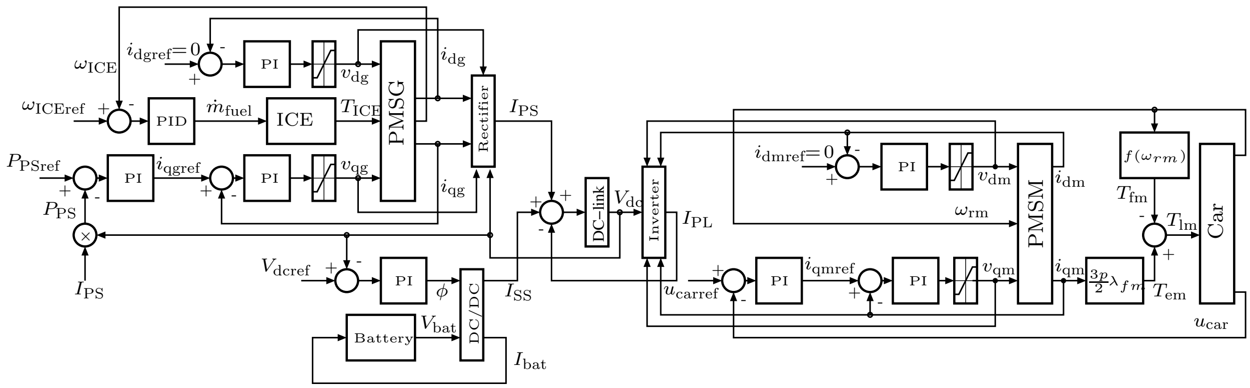

Figure 2: Block diagram showing the interconnection of the ICE, PMSG, rectifier, battery, DC/DC converter, inverter, PMSM and car, and the related control loops. Subscripts g, m and ref correspond to 'generator', 'motor' and 'reference'. The diagram provides an overview of the integrated control of the vehicle, but does not aim to comprehensively present and define the vehicle. Relevant variables are defined when used in this paper while details of the full model are available in [25].

Load (PL) and is powered by a Primary Source of energy (PS) and a Secondary Source of energy (SS), all connected to a common DC bus from which energy transfer takes place. The PS consists of a turbocharged 2.0L diesel ICE, mechanically coupled to a Permanent Magnet Synchronous Generator (PMSG) which is electrically connected to a three-phase rectifier. The SS contains a lithium-ion battery connected to a bi-directional DC-DC converter. Regenerative braking is possible by the PMSM behaving as a PMSG while capturing the kinetic energy from the wheels and converting it to electrical energy, which then gets stored in the SS. The interaction of the three branches and the overall component control scheme are shown in Fig. 2. The role of the SCS is to determine the two signals at the far left of the diagram: the reference power for the PS (P_{PSref}) and the reference speed of the ICE (ω_{ICEref}). The vehicle reference forward speed (u_{carref}) is set according to the speed profile the vehicle is desired to follow, and in the present work the DC bus voltage reference (V_{dcref}) is set to be constant at 700 V.

3. Powertrain Efficiency Analysis

To facilitate the SCS in deciding how to manage the energy sources, it is important that the powertrain efficiencies are well understood. This section will begin by analysing the PS followed by the SS, before formulating the unified overall powertrain efficiency.

3.1. Primary Source of Energy

The PS consists of three components and its overall efficiency can be determined by studying the component efficiencies. The energy of the PS originates from the fuel powering the ICE, where the chemical energy is converted to mechanical energy. The efficiency of this process is defined by

$$\eta_{ICE} = \frac{T_{ICE}\omega_{ICE}}{\dot{m}_f \cdot Q_{HV}}, \qquad (1)$$

where T_{ICE} and ω_{ICE} are the torque and speed of the ICE respectively, $\dot{m}_f$ is the fuel mass flow rate and Q_{HV} is the lower heating value of the fuel. The PS then uses the PMSG to convert the above to electrical energy, and the efficiency of this process is given by

$$\eta_g = \frac{\frac{3}{2}(v_{qg}i_{qg} + v_{dg}i_{dg})}{T_{ICE}\omega_{ICE}}, \qquad (2)$$

where v_{dg}, i_{dg}, v_{qg} and i_{qg} represent d-q voltages and currents respectively corresponding to the three-phase output of the PMSG. Lastly, the energy flows through the rectifier at a fixed efficiency of $\eta_{rec} = 94.6\%$ [26]. The overall energy of the PS is therefore defined as the product of these three efficiencies

$$\eta_{PS} = \eta_{ICE}\eta_g\eta_{rec} = \frac{\frac{3}{2}(v_{qg}i_{qg} + v_{dg}i_{dg}) \cdot \eta_{rec}}{\dot{m}_f \cdot Q_{HV}} \qquad (3)$$

which can be simplified and expressed as

$$\eta_{PS}(P_{PS}, \omega_{ICE}) = \frac{P_{PS}}{\dot{m}_f(P_{PS}, \omega_{ICE}) \cdot Q_{HV}}, \qquad (4)$$

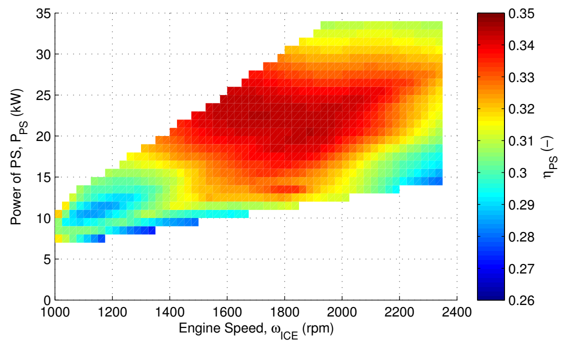

Figure 3: PS efficiency, η_{PS}, for varying PS power demand, P_{PS}, and engine speed, ω_{ICE}.

in which P_{PS} is the PS power at the DC-link.

Thus, for any given P_{PS} the efficiency η_{PS} can be determined by measuring the fuel rate $\dot{m}_f$, which will not only depend on P_{PS} but also ω_{ICE}. To investigate the impact of these variables on the PS efficiency for any given power demand, a test-model is used to load the PS with a varying amount of power for a certain engine speed (ω_{ICE}) to measure the generated power together with the fuel consumption under steady-state conditions. Tests are performed for power demands from $P_{PSmin} = 0$ kW to $P_{PSmax} = 34$ kW in 1 kW increments and engine speeds from 1000 RPM to 2275 RPM in 25 RPM increments. The results (Fig. 3) demonstrate that the PS is generally more efficient at higher levels of power demand and that the maximum efficiency is found at 22 kW at 1700 RPM. It is worth noting that there is a local maximum at 20 kW at 1900 RPM as well. This dual maxima phenomenon occurs due to the superpositioning of the dynamics of the ICE and PMSG. The envelope of the efficiency map is determined by feasibility of the ICE. The omitted data points at very low power requirements are either not operationally feasible or the model is not validated in that range. Furthermore, the engine has an internal control constraint for the air fuel ratio that essentially limits the power output at any engine speed, in order to reduce emissions [25].

In can be noted in (4) that the expression for η_{PS} is a function of ω_{ICE} as well as P_{PS}. However, with the obtained efficiency map in Fig. 3 we can now determine the optimal ω_{ICE} for a given P_{PS} such that η_{PS} is maximized. This relationship, as shown in Fig. 4 is independent of any choice by the SCS and can therefore be used in the optimization

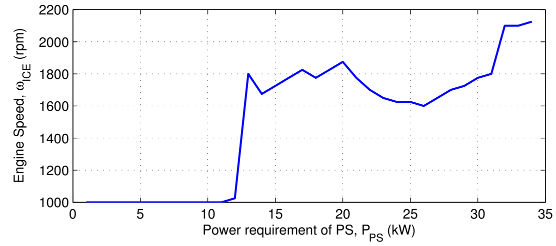

Figure 4: Engine speed ω_{ICE} for varying power requirements of the PS, P_{PS}, for maximum PS efficiency.

problem. The expression for η_{PS} can thus simply be expressed as

$$\eta_{PS}(P_{PS}) = \frac{P_{PS}}{\dot{m}_f(P_{PS}) \cdot Q_{HV}}. \qquad (5)$$

3.2. Secondary Source of Energy

Strictly speaking, the SS is an energy buffer, rather than an energy source. It receives energy from the PS either directly (by charging) or indirectly (by regenerative braking). It is therefore not straightforward to express the efficiency as an instantaneous value. The conventional approach is to express it as the energy charge-discharge efficiency[27], defined as

$$\eta_{bat,c-d} = \frac{E_{discharge}}{E_{charge}}, \qquad (6)$$

where the two energies are defined for the same SOC. Other alternatives include the expression of efficiency as the coulombic efficiency or the voltaic efficiency [28]. However, they all suffer from an inaccuracy: the underlying assumption of these types of efficiency is that the battery will be charged and discharged at the same power level. Consequently, when evaluating the efficiency of the battery at a discharge of, e.g. 10 kW as compared to 20 kW, it is not the actual instantaneous efficiency being compared, but rather it is a comparison with two different assumptions being made for the two cases. The assumptions are that the battery was charged with 10 kW in the past if discharging at 10 kW, and 20 kW if discharging at 20 kW. Clearly the past charging should be already fixed, and not determined by present and future discharging levels. To address this, the efficiency is separated into charging efficiency and discharging efficiency, where the former is defined as

$$\eta_{bat,c} = \frac{P_{bat-charge}}{P_{bat-in}} = \frac{V_{bat,OC} \cdot I_{bat}}{V_{bat} \cdot I_{bat}} = \frac{V_{bat,OC}}{V_{bat}}, \tag{7}$$

in which $P_{bat-charge}$ is the rate at which energy is being stored in the battery. This power is obtained by multiplying the current, I_{bat}, with the open-circuit voltage of the battery, $V_{bat,OC}$. P_{bat-in} corresponds to the power sent to the battery at its ports, while V_{bat} is the voltage at the same ports. Similarly the discharging efficiency can be formulated as

$$\eta_{bat,d} = \frac{P_{bat-out}}{P_{bat-discharge}} = \frac{V_{bat} \cdot I_{bat}}{V_{bat,OC} \cdot I_{bat}} = \frac{V_{bat}}{V_{bat,OC}}, \tag{8}$$

where $P_{bat-out}$ is the power delivered by the battery at its ports, and $P_{bat-discharge}$ is the power consumed by the battery internally. The latter power is obtained by multiplying the current with the open-circuit voltage of the battery.

As the objective is to eventually compare the efficiency of the PS and SS, it is not sufficient to only consider the discharging efficiency of the SS as it neglects the future losses from replenishing the consumed SOC. This can be best addressed by including a correction factor η_{re} reflecting the average efficiency associated with the PS replenishing the SS. This correction factor could be estimated in real time during driving, but as its dynamics are very slow it is considered a constant (at 33%) for the purposes of this work. Also, the efficiency of the DC-DC converter is defined to be constant at $\eta_{dcdc} = 96\%$ [29]. Thus the overall efficiency of the SS can be expressed as

$$\eta_{SS} = \begin{cases} \frac{V_{bat,OC}}{V_{bat}}\eta_{dcdc} & P_{SS} < 0 \\ \frac{V_{bat}}{V_{bat,OC}}\eta_{re}\eta_{dcdc} & P_{SS} \geq 0 \end{cases}, \tag{9}$$

in which P_{SS} is the SS power at the DC-link.

To allow simplification of (9) and make it more usable for the optimization in the next section, battery voltage can be substituted with current. The battery voltage is modelled to be a function of I_{bat} and SOC. However, $V_{bat,OC}$ has $I_{bat} = 0$ so we can determine that $V_{bat,OC} = f(SOC)$. Similarly, I_{bat} is a function of SOC and V_{bat}, which can however be expressed as a function of P_{SS} as follows:

$$I_{bat} = \begin{cases} \frac{P_{SS} \cdot \eta_{dcdc}}{V_{bat}} & P_{SS} < 0 \\ \frac{P_{SS}}{V_{bat} \cdot \eta_{dcdc}} & P_{SS} \geq 0 \end{cases}. \tag{10}$$

Table 1: Parameter values of the Li-ion battery

Parameter	Symbol	Value
Fully charged voltage	V_{Full}	250.2572 V
Nominal Voltage	V_{nom}	215 V
Rated capacity	Q_{max}	20 Ah
Capacity at V_{nom}	Q_{nom}	18.087 Ah
Battery constant voltage	E_0	232.926 V
Polarization constant	K_1	0.06068 V/(Ah)
Polarization resistance	K_2	0.06068 Ω
Internal resistance	R_{bat}	0.1075 Ω
Time constant (I^*_{bat})	τ_r	30 s
Nominal discharge current	i_{nom}	8.6957 A
EZ amplitude	A	18.266 V
EZ time constant inverse	B	3.0531 (Ah)$^{-1}$

Now, by considering (9) and (10) the overall efficiency of the SS is given by

$$\eta_{SS} = \begin{cases} \frac{V_{bat,OC} I_{bat}}{P_{SS} \cdot v} & P_{SS} < 0 \\ \frac{P_{SS} \cdot v}{V_{bat,OC} I_{bat}} & P_{SS} \geq 0 \end{cases}, \tag{11}$$

where

$$v = \begin{cases} 1 & P_{SS} < 0 \\ \eta_{re} & P_{SS} \geq 0 \end{cases}. \tag{12}$$

The symmetry of η_{SS} in (11) allows the efficiency to be expressed as

$$\eta_{SS} = \begin{cases} 1/\eta^*_{SS} & P_{SS} < 0 \\ \eta^*_{SS} & P_{SS} \geq 0 \end{cases}, \tag{13}$$

where

$$\eta^*_{SS}(P_{SS}, SOC, I_{bat}) = \frac{P_{SS} \cdot v}{V_{bat,OC} I_{bat}}. \tag{14}$$

It's worth noting that the SS efficiency $\eta_{SS} \in [0, 1]$ for both $P_{SS} < 0$ and $P_{SS} \geq 0$, as is expected from an efficiency term. However, the term η^*_{SS} is not strictly speaking an efficiency, as it represents the inverse of the SS efficiency during charging operation ($P_{SS} < 0$), for which $\eta^*_{SS} \in [1, \infty]$ and therefore overall $\eta^*_{SS} \in [0, \infty]$. The expression of η^*_{SS} is used later to simplify the optimization process.

The defined SS efficiency can now be determined experimentally, analytically or through simulations. The methodology and results presented in [23] took the latter approach, so the analytical method will be presented in this paper.

Lithium-ion batteries are often modelled using equivalent electric circuits of varying orders [30].

The battery model used here [31] is a modified version of Shepherd's electrochemical equations that describe the battery dynamics using its physical parameters, offering higher accuracy. The model has been validated against experimental data and key parameters are given in Table 1. It has minor differences in dynamics between charging and discharging operation to account for differences in the polarization resistance. However, below only the discharging dynamics are presented, although the dynamics of each mode of operation were considered when performing the analysis and producing the efficiency map in this paper. The key discharging dynamic of the battery model is given by

$$V_{bat} = E_0 - \frac{Q_{max} \cdot K_1 Q}{Q_{max} - Q} - \frac{Q_{max} \cdot K_2 I^*_{bat}}{Q_{max} - Q} + Ae^{-B \cdot Q} - R_{bat} \cdot I_{bat}, \tag{15}$$

where the I^*_{bat} variable is a low-pass filtered version of I_{bat} flowing through the polarization resistance K_2; A and B are constants related to the Exponential Zone (EZ) as shown in Table 1; and Q represents the consumed charge and is related to SOC by

$$SOC = 1 - \frac{Q}{Q_{max}}. \tag{16}$$

To make the efficiency model time-invariant, it is assumed that $I^*_{bat} = I_{bat}$, so that we obtain the efficiencies for steady-state operation. To obtain $V_{bat,OC}$, (15) should be substituted with $I_{bat} = 0$ to create open circuit conditions. To express this as a function of SOC, we substitute with (16) to give

$$V_{bat,OC}(SOC) = E_0 - \frac{K_1 \cdot Q_{max}(1 - SOC)}{SOC} + Ae^{-B \cdot Q_{max}(1-SOC)}. \tag{17}$$

Lastly, I_{bat} can be determined by combining (10), (15) and (16) to produce the following quadratic equation

$$aI^2_{bat} + bI_{bat} + c = 0, \tag{18}$$

where

$$a = \frac{K_2}{SOC} + R_{bat},$$
$$b = \frac{K_1 Q_{max}(1 - SOC)}{SOC} - E_0 - Ae^{-B \cdot Q_{max}(1-SOC)},$$
$$c = \frac{P_{SS}}{\eta_{dcdc}}.$$

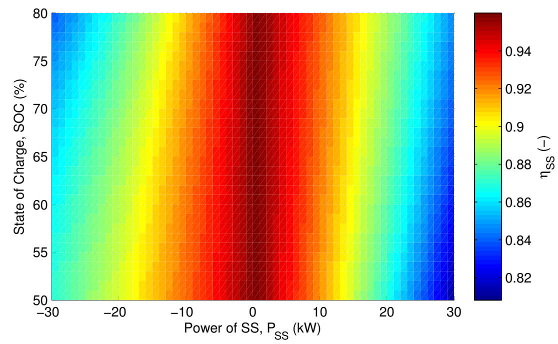

Figure 5: SS efficiency, η_{SS}, for varying charging (negative) and discharging (positive) SS power demand, P_{SS}, and SOC, using η_{re}=1.

Thus, we obtain the battery current as

$$I_{bat}(P_{SS}, SOC) = \frac{-b \pm \sqrt{b^2 - 4ac}}{2a}, \tag{19}$$

where it is only a function of P_{SS} and SOC. This allows the expression of (14) as follows:

$$\eta^*_{SS}(P_{SS}, SOC) = \frac{P_{SS} \cdot v}{V_{bat,OC} I_{bat}}. \tag{20}$$

Equations (17) and (19) are then iteratively solved for $SOC \in [0.50, 0.80]$ and $P_{SS} \in [-30, 30]$ kW in steps of 1% and 1 kW respectively before being substituted into (20) and then (13) to provide the efficiency of the SS. The obtained results are presented in Fig. 5.

As expected, the SS is most efficient at low magnitudes of power. Furthermore, it is interesting to note that the charging becomes slightly more efficient at lower SOC levels, while discharging becomes slightly more efficient at higher SOC levels. Thus, if efficient operation is encouraged, charge sustaining is indirectly taking place to a limited extent.

3.3. Total Efficiency

Having obtained the efficiencies for both the PS and the SS in (5) and (11) respectively, the combined total efficiency (for $P_{PS} + P_{SS} > 0$) can be expressed as

$$\eta_{tot} = \begin{cases} \frac{P_{PS}+P_{SS}}{P_{PS}/\eta_{PS}+P_{SS}\cdot\eta_{SS}} & P_{SS} < 0 \\ \frac{P_{PS}+P_{SS}}{P_{PS}/\eta_{PS}+P_{SS}/\eta_{SS}} & P_{SS} \geq 0 \end{cases}, \tag{21}$$

which can be simplified using (13) to

$$\eta_{tot} = \frac{P_{PS} + P_{SS}}{P_{PS}/\eta_{PS} + P_{SS}/\eta^*_{SS}}. \tag{22}$$

To simplify further, the individual powers of the sources can be expressed as a fraction of P_{PL}, the total power requested by the PL, according to

$$u = \frac{P_{PS}}{P_{PL}}, \tag{23}$$

$$P_{PS} + P_{SS} = P_{PL}, \tag{24}$$

giving a single decision variable u (for $P_{PL} > 0$) to determine both P_{PS} and P_{SS}. Thus the total efficiency can be formulated as

$$\eta_{tot}(u, P_{PL}, SOC) = \frac{\eta_{PS}\eta_{SS}^{*}}{\eta_{PS}(1-u) + \eta_{SS}^{*}u}. \tag{25}$$

4. Supervisory Control Systems

Having obtained expressions for the total efficiency of the energy sources, intelligent decisions can be made by the SCS. This section presents the novel Efficiency Maximizing Map (EMM) control strategy that utilizes the previous analysis to maximize the efficiency at any given time. This is followed by the improved Efficiency Maximizing and Charge Sustaining Map (EMCSM) control that goes a step further to operate in a charge sustaining fashion. Finally, two separate conventional control schemes are introduced for benchmarking purposes. These are only covered briefly as they have been described more thoroughly in the referenced papers.

4.1. Efficiency Maximizing Map Control

The fundamental principle of the EMM control is to operate the energy sources such that the efficiency η_{tot} is maximized. As it is clear from the definition of this variable in the previous sub-section, it depends on two defined variables (P_{PL} and SOC) and one decision variable (u). The objective is thus to produce a map for the optimal decision variable given the defined variables, according to

$$EMM : [u_{opt}] = f(P_{PL}, SOC). \tag{26}$$

The optimization problem can be formulated as

$$P_{EMM} \begin{cases} \max\limits_{u} \eta_{tot} \\ 0 \leq u \leq \frac{P_{PSmax}}{P_{PL}} \end{cases} \tag{27}$$

and can be solved through a simple iterative process using exhaustive search within the search space of $SOC \in [0.50, 0.80]$, $P_{SS} \in [-30, 30]$ kW and $P_{PS} \in [0, 34]$ kW. Note that the search for $\omega_{ICE} \in$

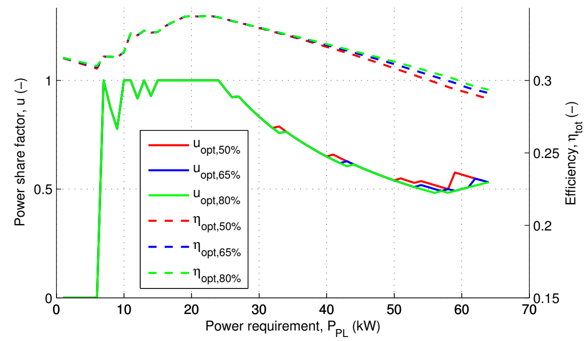

Figure 6: Optimal power share u_{opt} and corresponding total efficiency η_{tot} for varying power requirement P_{PL} at SOC levels of 50%, 65% and 80% (as given in legend).

$[1000, 2225]$ RPM is not needed due to the precomputation of $\omega_{ICE,opt} = f(P_{PS})$ as shown in Fig. 4, thus significantly reducing computational time (which is not a significant issue, as optimization is performed off-line). The efficiency is therefore computed for every feasible combination of values for the defined and the decision variables and the optimal u is selected in each case (the range of u is set by the P_{PL} of interest and P_{PSmax} (34 kW) and is appropriately discretized). Note that the optimization is only performed for $P_{PL} > 0$ as the optimal control input is trivial ($u = 0$) during regenerative braking. Once this optimization is performed, the EMM control map is obtained.

The optimal power share factor u_{opt} with varying power demand is shown in Fig. 6 together with the realized efficiency η_{tot}. It can be seen that the SCS chooses to operate SS-only mode during low P_{PL} and almost PS-only mode during mid-range P_{PL}. For higher power requirements the EMM control uses a blended mode to drive the powertrain. It's worth noting that the dependence of u_{opt} on SOC-levels is quite limited, as could be expected from the efficiency plot of the SS in Fig. 5. The total efficiency η_{tot} that is realized by this selection of u is quite steady above 30% for most power requirements.

As mentioned in Section 3.2, the replenishing efficiency η_{re} has been fixed as a constant at 33%, which corresponds to the typical efficiency of the PS, as shown in Fig. 3. To confirm this value, and to demonstrate its limited sensitivity to driving cycles, simulations are run for three driving cycles to compare the resulting fuel economy. Results for equivalent fuel consumption m_{eq} (defined later in

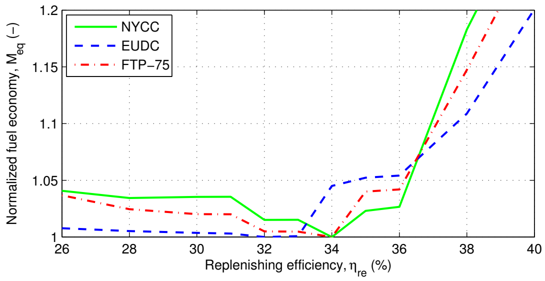

Figure 7: Normalized fuel economy for varying selections of η_{re} for the factor v. $M_{eq} = 1$ corresponds to the minimum equivalent fuel consumption for each driving cycle.

Section 5.3) are normalized as follows:

$$M_{eq} = \frac{m_{eq}}{m_{eq,min}}, \tag{28}$$

where $m_{eq,min}$ corresponds to the minimum equivalent fuel consumption obtained for a given driving cycle. These results are shown in Fig. 7. As can be seen, the optimal range of η_{re} is around 32-34% for all driving cycles, just before the knee of the graph at 35% that corresponds to the maximum efficiency of the PS.

4.2. Efficiency Maximizing and Charge Sustaining Map Control

The EMM control has no inherent constraints in terms of SOC, so the battery could end up depleted or overcharged and permanently damaged. To address this, a charge sustaining factor k is included in the control design, which encourages the battery to be charged at low SOC values and discharged at high SOC values. This bias is introduced in the expression of total efficiency, by weighting the input power of the SS as follows:

$$\eta_{CS}(u, P_{PL}, SOC) = \frac{\eta_{PS}\eta^*_{SS}}{\eta_{PS}(1-u) + k\eta^*_{SS}u}. \tag{29}$$

For $k > 1$, the SS discharging power becomes heavier, causing it to be reduced by the optimization algorithm. Simultaneously the SS charging power becomes heavier, but since it is a negative quantity, this actually encourages further charging of the battery (as $\dot{m}_f$ is always positive and we are aiming to minimize the denominator). Conversely, for smaller k values, the discharging of the SS becomes more attractive and charging less desirable. The new objective is not only to maximize the efficiency but also to keep the SOC levels within a

Table 2: Definition of charge sustaining factor k

$k(SOC\%)$	Defined such that
$k(80)$	$u = 0$ for $P_{PL} \leq P_{SSmax}$
$k(75)$	$1 - (1 - k(80))/4$
$k(70)$	No correction
$k(60)$	No correction
$k(55)$	$1 + (k(50) - 1)/4$
$k(50)$	$u \geq 1$ for $0 < P_{PL} \leq P_{PSmax}$

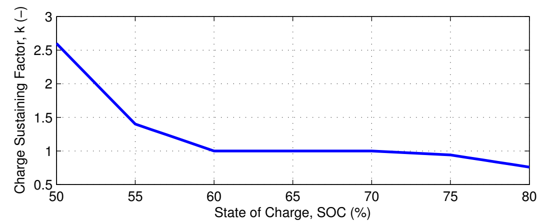

Figure 8: Charge sustaining factor, k, as a function of SOC.

certain range. The upper limit of SOC in this case has been chosen to be 80% to allow a buffer for regenerative braking, as well as to avoid very high SOC that accelerates degradation of the battery. Similarly a lower limit of 50% is chosen to limit the depth of discharge to 30%, as it is exponentially related to battery degradation. Thus, the new optimization problem to be solved can be expressed as

$$P_{EMCSM} \begin{cases} \max\limits_{u} \eta_{CS} \\ 0 \leq u \leq \frac{P_{PSmax}}{P_{PL}} \\ 0.50 \leq SOC \leq 0.80 \end{cases}. \tag{30}$$

To ensure operation within this SOC range the charge sustaining factor k is shaped according to the rules presented in Table 2. During operation at high SOC, the PS is used to a minimal extent while at lower SOC the PS is often charging the SS. The resultant profile for the charge sustaining factor k is shown in Fig. 8. It can be seen that the lower values of SOC are associated with a high k value, encouraging the SCS to charge the battery, as discussed above. Similarly, at high SOC values, the k value is low and thus encourages the battery to be discharged. There is a flat region between 60% and 70% where no modification is desired.

This charge sustaining factor is implemented and new maps are produced for optimal power share factor u_{opt} and total efficiency η_{tot} in Figs. 9 and 10 respectively. Clearly the power share factor is consistently higher for lower SOC (often larger than one) and quite low (often zero) for higher SOC. The charge sustaining factor thus seems successful in maintaining the SOC within the desired thresholds and the resulting power share is in accordance with the rules defined in Table 2. However, it is clear from Fig. 10 that this charge sustaining correction comes at the expense of efficiency in the case of extreme SOC values. Arguably, it is better to suffer some reduced efficiency immediately rather than damaging the battery or for that matter suffer heavy inefficiency later. Thus, over longer periods of driving, the EMCSM could be more efficient.

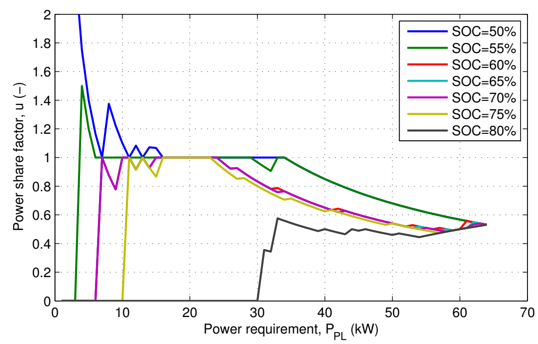

Figure 9: Power share factor u_{opt} for varying power requirement P_{PL} and SOC, with charge being sustained.

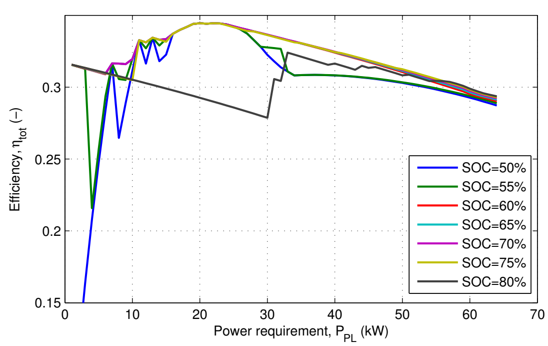

Figure 10: Total efficiency η_{tot} for varying power requirement P_{PL} and SOC, with charge being sustained.

4.3. Thermostat Control Strategy

The Thermostat Control Strategy (TCS) is a simple, robust SCS that achieves a good fuel economy [32, 33]. It is the most conventional control strategy for series HEVs and is a suitable benchmark for the EMM and EMCSM control. The basic principle is to run the PS at its optimal point and have the SS act as an equalizer, as

$$P_{SS} = P_{PL} - P_{PS,opt} \tag{31}$$

where $P_{PS,opt}$ is defined to be at 22 kW at 1700 RPM as shown in Fig. 3. This mode of operation is valid until the SOC reaches its upper threshold ($SOC_U = 80\%$), at which point it enters a mode of SS-only operation. This mode quickly depletes the SS and once the SOC hits the lower threshold ($SOC_L = 50\%$) it returns to operate the PS at its optimal point. This logic is implemented by $S(t)$, which is the state determining whether the engine-generator set is active ($S(t) = 1$) or not ($S(t) = 0$):

$$S(t) = \begin{cases} 0 & SOC(t) \geq SOC_U \\ S(t^-) & SOC_L < SOC(t) < SOC_U . \\ 1 & SOC(t) \leq SOC_L \end{cases} \tag{32}$$

For the purpose of stable operation an additional rule is also introduced: the PS reduces its supply of power to a minimum level ($P_{PSmin} = 7$ kW) during the event of regenerative braking, to avoid overcharging the battery.

4.4. Power Follower Control Strategy

As an alternative to the TCS the series HEV is often equipped with a Power Follower Control Strategy (PFCS) [8, 33]. Rather than using the ICE at its most efficient point of operation, the PFCS generally has the PS follow the load of the PL, with some consideration for the SOC. When the load from the motor (P_{PL}) is low and SOC is high, the SS is selected to deliver the power to the vehicle ($S(t) = 0$). Conversely, when P_{PL} is high or SOC is low, the PS is selected to meet the load ($S(t) = 1$). These states are defined as shown in Fig. 11.

For $S(t) = 0$, we always have $P_{PS} = 0$. For $S(t) = 1$, the operation of the PS is defined as

$$P_{PS}(t) = \begin{cases} P_{PSmin} & SOC(t) \geq SOC_U \\ P_m(t) & SOC_L < SOC(t) < SOC_U \\ P_{PSmax} & SOC(t) \leq SOC_L \end{cases} \tag{33}$$

where P_m is given by

$$P_m(t) = P_{PL} + P_{ch}\left[\frac{SOC_U + SOC_L}{2} - SOC(t)\right]. \tag{34}$$

As shown, the PS is essentially following the load PL when the SOC is at the midpoint between SOC_L and SOC_U, but biases the operation in

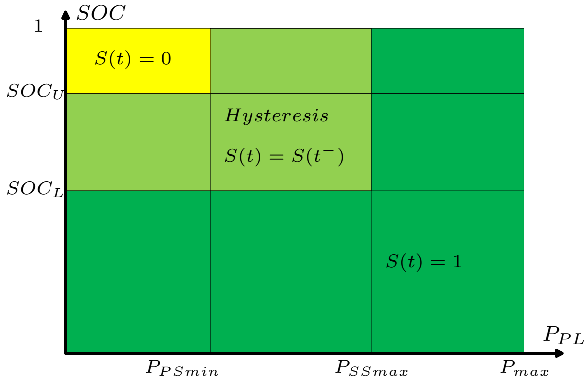

Figure 11: The PFCS operates in two different states, depending on given SOC and P_{PL}, and has an area of hysteresis in between. Here, $P_{max} = P_{PSmax} + P_{SSmax}$.

favour of charging or discharging the SS in the cases of low and high SOC respectively. The bias is scaled by P_{ch} which is tuned to optimise fuel economy ($P_{ch} = 0.5$ in this work). Note that in general $P_{SS} \neq 0$ when $S(t) = 1$.

5. Results

The implemented SCS can now be simulated to investigate operation and performance. Simulations are run for three different driving cycles: the NYCC is low-speed urban driving; the EUDC is European highway driving; and FTP-75 combines urban and high-speed driving.

5.1. Power Profiles

The EUDC cycle is relatively short and shows most clearly the mode of operation of the SCS, so only the power profiles of this driving cycle are presented here. Also, the operation of the EMM and EMCSM are practically identical when observing the power profiles, so only EMCSM is shown. Figs. 12, 13 and 14 illustrate the power time histories for the PS, SS and PL for the TCS, PFCS and EMCSM control respectively. As the TCS and PFCS operate in two very distinct modes which require a slightly longer timeframe to observe, results have been presented for two consecutive iterations of the EUDC driving cycle.

The first 280 seconds of the TCS are powered fully by the SS, requiring close to the maximum power rating of the battery. Thereafter the PS is switched on and provides 22 kW constantly, which

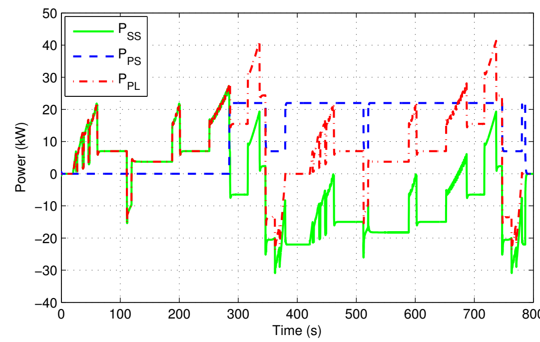

Figure 12: Power time histories for PS, SS and PL for the EUDC driving cycle when the TCS is used.

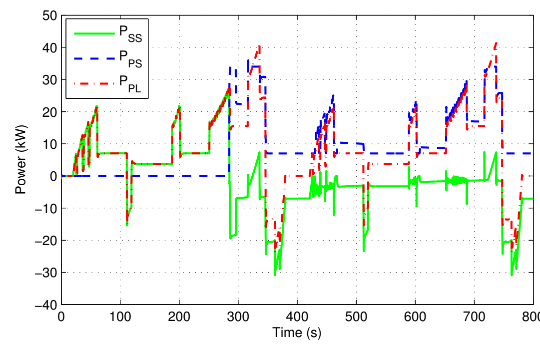

Figure 13: Power time histories for PS, SS and PL for the EUDC driving cycle when the PFCS is used.

is its optimal point of operation. There are occasional dips in power from the PS during regenerative braking, to ensure the SS is not overloaded. During this second stage of operation, the battery is almost always being intensively charged, apart from the occasions where required power P_{PL} exceeds the optimal point of operation of the PS.

Similarly, the PFCS opens by operating with SS only, but soon enters its hybrid mode. During cruising at lower speeds (<7 kW) the PS operates steadily at minimum power, while during accelerations and high-speed cruising the PS ends up providing all the power apart from during times of fast transitions or power requirements in excess of the maximum ratings of the PS (34 kW). The PS power profile is essentially following the PL power, but there is an offset (that is proportional to the SOC deviation) that decreases with progression into the driving cycle.

Lastly, the EMCSM control is applying the efficiency maximizing power share factor as derived in

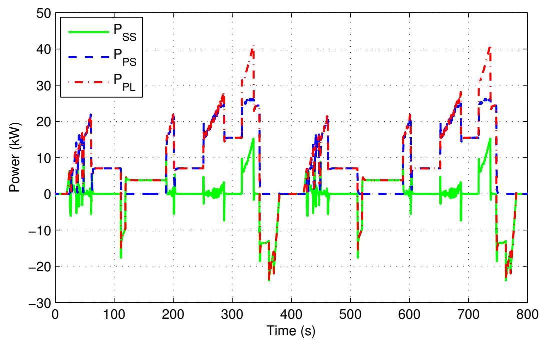

Figure 14: Power time histories for PS, SS and PL for the EUDC driving cycle when the EMCSM control is used.

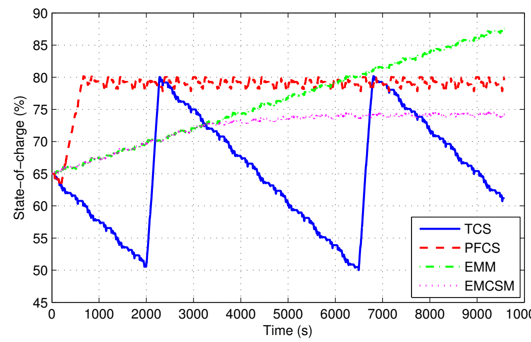

Figure 15: SOC time histories for the NYCC driving cycle for the four presented control systems.

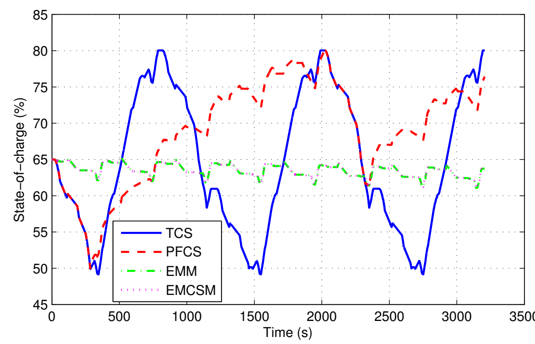

Figure 16: SOC time histories for the EUDC driving cycle for the four presented control systems.

the previous section. The EMCSM control finds it more efficient to use the PS for cruising at lower speeds as well and also avoids pushing the PS to very high power levels. The EMCSM is thus the most conservative in terms of using the SS (quite often $P_{SS} = 0$), which is also beneficial for the health and longevity of the battery.

5.2. State-of-Charge Profiles

In addition to studying the power profiles for the different SCSs it is interesting to compare their SOC profiles, which are presented in Figs. 15, 16 and 17 for the three driving cycles. As SOC is a quite slow dynamic, results for repeated driving cycles have been presented (16x NYCC, 8x EUDC and 4x FTP-75).

The nature of the TCS is very apparent in the zigzagging between the SOC boundaries, as the battery is alternately charging and discharging. The high-speed driving of the EUDC produces almost a triangle wave as the charging and discharging powers are quite persistent and balanced. However, as the NYCC and FTP-75 driving cycles are often operating at zero or low powers, the charging of the battery is very rapid when the PS produces 22 kW. This results in the SOC profiles looking more like a sawtooth wave. Similarly, the PFCS also tends to behave in an oscillating fashion due to its operation in two distinct states, where $S(t) = 0$ often leads to discharging patterns similar to the TCS (for EUDC and FTP-75 in particular). However, the charging is significantly less aggressive, as seen in the previous sub-section, leading to a decrease in the amplitude (or frequency) of the oscillations.

However, the EMM control does not oscillate and instead drifts away from the initial SOC (although at a very slow pace for the EUDC) but is not constrained to any particular SOC range. Therefore, the SOC can be seen to exceed 80% which is not desirable as discussed previously in Section 3.2. This is however addressed by EMCSM which can be seen to follow the EMM profile until the SOC exceeds 70% and thereafter it begins saturating. As none of the driving cycles are very aggressive the saturation is around 74% (rather than closer to 80%).

5.3. Fuel Economy

The fuel consumption and the final SOC for each driving cycle (again for 16x NYCC, 8x EUDC and 4x FTP-75) and control strategy are presented in Table 3, together with the equivalent fuel consumption m_{eq}. The fuel economy is evaluated by comparing m_{eq}, which considers the shortage/surplus of final SOC. Many analytical methods have been described in defining such an equivalence between SOC and fuel consumption [34, 27, 35]. This paper has used the mapping of data from the efficiency

Table 3: Comparison of Fuel Economy

	16x NYCC				8x EUDC				4x FTP-75			
	TCS	PFCS	EMM	EMCSM	TCS	PFCS	EMM	EMCSM	TCS	PFCS	EMM	EMCSM
Fuel [kg]	0.863	1.123	0.975	0.828	2.164	2.130	1.823	1.823	1.980	2.170	1.983	1.911
SOC [%]	61.20	80.02	87.56	74.20	80.04	76.39	63.74	63.74	53.96	72.23	79.66	73.69
m_{eq} [kg]	0.916	0.967	0.741	0.732	2.001	2.012	1.840	1.840	2.132	2.095	1.831	1.821
Δm_{eq} [%]	0	+5.6%	-19.1%	-20.0%	0	+2.2%	-8.3%	-8.3%	0	-1.7%	-14.1%	-14.6%

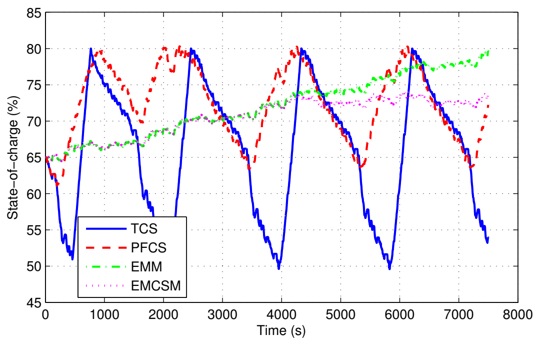

Figure 17: SOC time histories for the FTP-75 driving cycle for the four presented control systems.

analysis presented in Section 3, and considered how much fuel would be consumed/saved in bringing the SS back to its initial SOC. Of course, in reality there is no constraint such that the final SOC needs to be same as the initial SOC as during real driving there would be a mix of varying types of driving and it is often beneficial to store surplus charge in the battery. However, to ensure fair evaluation of fuel economy, this is needed.

If the final SOC exceeds the initial SOC, this can be considered as the SS having been charged too much or being discharged to little. The former approach is chosen, but the optimal approach would depend on the driving cycle. One of the most common points of operation for the PS when charging the SS is at 22 kW. If the PS instead operates at 21 kW for some of these times, and thus charges the battery with 1 kW less, then some fuel would be saved and when done enough could bring the final SOC in alignment with the initial SOC. Thus the equivalency between fuel and SOC during surplus charge can be defined as

$$s_c = \frac{\dot{m}_{f,22} - \dot{m}_{f,21}}{I_{bat,1}} \cdot 72,000 \qquad (35)$$

where the subscripts 1, 21 and 22 signify the point of operation for the PS and SS and the factor of 72,000 (as $Q_{max} = 20 \cdot 3600As$) is used to convert the units from kg/As to kg per unit SOC.

For the case of the final SOC being less than the initial SOC, the same approach could be used, but a more precise method would be to consider the case of the PS charging the SS at its optimal point at the end of the driving cycle (the vehicle being stationary). Thus no assumptions need to be made with respect to the driving schedules. This approach produces the following equivalency between fuel and SOC during shortage of charge:

$$s_d = \frac{\dot{m}_{f,22}}{I_{bat,22}} \cdot 72,000. \qquad (36)$$

These two expressions provide us with $s_c = 1.04$ kg/SOC and $s_d = 1.38$ kg/SOC that are used to determine the total equivalent fuel as follows:

$$m_{eq} = \begin{cases} m_f + s_c \cdot \Delta SOC & \Delta SOC < 0 \\ m_f + s_d \cdot \Delta SOC & \Delta SOC > 0 \end{cases}, \qquad (37)$$

where $\Delta SOC = SOC_{initial} - SOC_{final}$. There are more accurate methods to estimate s_c and s_d but these are more complex and driving cycle sensitive. The presented method is sufficient for the purposes of this work and the possible error in overall fuel economy has been mitigated by comparing results from repeated driving cycles.

The simulation results and the computed m_{eq} are presented in Table 3, together with Δm_{eq} which shows the percentage difference compared to the TCS. The EMCSM control is achieving an improvement of about 8% for high way driving, about 20% for urban driving, and 15% for mixed driving as compared to TCS. The improvement over the PFCS is even larger, apart from the FTP-75 driving cycle. The EMCSM control performs marginally better than the EMM control, despite (as was discussed in Section 3.2) the instantaneous optimality of operation being compromised to maintain the battery within the desired range of SOC. This is explained by the long-term benefits of operating in a more efficient SOC-region of the battery as well as the reduced number of engine-start events. In the case of NYCC, the EMM control exceeds the desired range of SOC and reaches 87.56%, while the EMCSM saturates around 74.20%. However, in the case of EUDC, the fuel economy of EMM and EMCSM are identical as the SOC never deviates enough from the initial SOC to require any charge-sustaining modification (it always remains between 60% and 70%). The fuel economy results are also shown visually in Fig. 18.

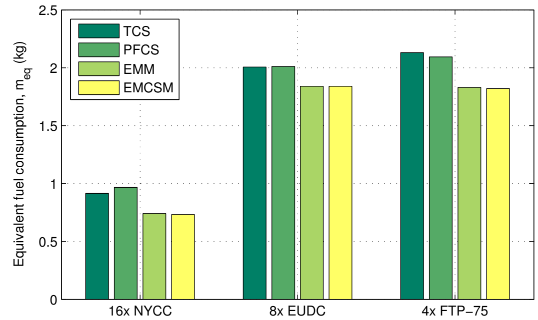

Figure 18: Comparison of equivalent fuel consumption for TCS, PFCS, EMM and EMCSM for repeated iterations of the three driving cycles.

6. Conclusions

A SCS that maximizes the powertrain efficiency has been proposed in this paper. To obtain the overall powertrain efficiency, the component efficiencies of the ICE, generator, rectifier, battery and DC-DC converter are considered. The study dived particularly deep into the battery efficiency compared to past work and considered charging and discharging efficiencies separately. The overall efficiency of the powertrain was then expressed as a single expression that it optimized off-line to produce a control map. This map takes the load request of the PL and the SOC of the battery as inputs in real-time and provides the optimal power share factor u_{opt} as output, directly determining the power supply of the PS and SS. To ensure charge sustaining operation, a weight factor was introduced to bias the powertrain in favour of charging the battery during states of low SOC and discharging the battery at high SOC.

Simulation results for three diverse driving cycles have been obtained using a dynamical, physics-based series HEV model to show stable, healthy and efficient operation. The EMCSM control outperformed the TCS and PFCS control strategies by about 15% and 13% respectively in fuel economy for mixed driving which is similar or better than most ECMS results in literature. Furthermore, the study of power and SOC profiles show the EMCSM to be significantly less aggressive on the battery compared to the other SCSs. This affects both the safety and longevity of the battery.

[1] N. Tanaka, et al., Technology roadmap: Electric and plug-in hybrid electric vehicles, International Energy Agency, Tech. Rep (2011).

[2] New Automotive Innovation and Growth Team, An independent report on the future of the automotive industry in the UK, London: BERR (2009).

[3] X. Mosquet, M. Devineni, T. Mezger, et al., Powering autos to 2020: the era of the electric car, Boston Consulting Group (2011).

[4] C. Hou, M. Ouyang, L. Xu, H. Wang, Approximate pontryagins minimum principle applied to the energy management of plug-in hybrid electric vehicles, Applied Energy 115 (2014) 174–189.

[5] K. Çagatay Bayindir, M. A. Gözüküçük, A. Teke, A comprehensive overview of hybrid electric vehicle: Powertrain configurations, powertrain control techniques and electronic control units, Energy Conversion and Management 52 (2011) 1305 – 1313.

[6] L. V. Pérez, E. A. Pilotta, Optimal power split in a hybrid electric vehicle using direct transcription of an optimal control problem, Mathematics and Computers in Simulation 79 (2009) 1959–1970.

[7] D. Crolla, Q. Ren, S. ElDemerdash, F. Yu, Controller design for hybrid vehicles - state of the art review, in: Vehicle Power and Propulsion Conference (VPPC), 2008, pp. 1–6.

[8] F. Salmasi, Control strategies for hybrid electric vehicles: Evolution, classification, comparison, and future trends, IEEE Transactions on Vehicular Technology 56 (2007) 2393–2404.

[9] X. He, M. Parten, T. Maxwell, Energy management strategies for a hybrid electric vehicle, in: Vehicle Power and Propulsion Conference (VPPC), 2005, pp. 390–394.

[10] R. M. Patil, Z. Filipi, H. K. Fathy, Comparison of supervisory control strategies for series plug-in hybrid electric vehicle powertrains through dynamic programming, IEEE Transactions on Control Systems Technology (2014).

[11] C.-C. Lin, H. Peng, J. W. Grizzle, J.-M. Kang, Power management strategy for a parallel hybrid electric truck, IEEE Transactions on Control Systems Technology 11 (2003) 839–849.

[12] X. Hu, L. Johannesson, N. Murgovski, B. Egardt, Longevity-conscious dimensioning and power management of the hybrid energy storage system in a fuel cell hybrid electric bus, Applied Energy (2014).

[13] T. Nüesch, P. Elbert, M. Flankl, C. Onder, L. Guzzella, Convex optimization for the energy management of hybrid electric vehicles considering engine start and gearshift costs, Energies 7 (2014) 834–856.

[14] S. Boyd, L. Vandenberghe, Convex optimization, Cambridge university press, 2009.

[15] L. Serrao, S. Onori, G. Rizzoni, ECMS as a realization of pontryagin's minimum principle for HEV control, in: American Control Conference (ACC), IEEE, 2009, pp. 3964–3969.

[16] G. Paganelli, S. Delprat, T.-M. Guerra, J. Rimaux, J.-J. Santin, Equivalent consumption minimization strategy for parallel hybrid powertrains, in: Vehicular Technology Conference (VTC), volume 4, IEEE, 2002, pp. 2076–2081.

[17] J. Torres, R. Gonzalez, A. Gimenez, J. Lopez, Energy management strategy for plug-in hybrid electric vehicles. a comparative study, Applied Energy 113 (2014) 816–824.

[18] D. Feroldi, M. Serra, J. Riera, Energy management strategies based on efficiency map for fuel cell hybrid vehicles, Journal of Power Sources 190 (2009) 387–401.

[19] N. J. Schouten, M. A. Salman, N. A. Kheir, Energy management strategies for parallel hybrid vehicles using fuzzy logic, Control Engineering Practice 11 (2003) 171–177.

[20] L. Damiani, M. Repetto, A. P. Prato, Improvement of powertrain efficiency through energy breakdown analysis, Applied Energy 121 (2014) 252–263.

[21] X. Hu, N. Murgovski, L. Johannesson, B. Egardt, Energy efficiency analysis of a series plug-in hybrid electric bus with different energy management strategies and battery sizes, Applied Energy 111 (2013) 1001–1009.

[22] V. Sezer, M. Gokasan, S. Bogosyan, A novel ECMS and combined cost map approach for high-efficiency series hybrid electric vehicles, IEEE Transactions on Vehicular Technology 60 (2011) 3557–3570.

[23] W. Shabbir, S. A. Evangelou, Efficiency maximizing and charge sustaining supervisory control for series hybrid electric vehicles, in: Conference on Decision and Control (CDC), IEEE, 2012, pp. 6327–6332.

[24] W. Shabbir, C. Arana, S. A. Evangelou, Series hybrid electric vehicle supervisory control based on off-line efficiency optimization, in: International Electric Vehicle Conference (IEVC), IEEE, 2012, pp. 1–5.

[25] S. A. Evangelou, A. Shukla, Advances in the modelling and control of series hybrid electric vehicles, in: American Control Conference (ACC), IEEE, 2012, pp. 527–534.

[26] M. Shen, A. Joseph, J. Wang, F. Z. Peng, D. J. Adams, Comparison of traditional inverters and Z-source inverter for fuel cell vehicles, IEEE Transactions on Power Electronics 22 (2007) 1453–1463.

[27] L. Guzzella, A. Sciarretta, Vehicle propulsion systems, 2 ed., Springer, 2007.

[28] G. M. Masters, Renewable and efficient electric power systems, John Wiley & Sons, 2005.

[29] M. Pahlevaninezhad, P. Das, J. Drobnik, P. K. Jain, A. Bakhshai, A novel ZVZCS full-bridge DC/DC converter used for electric vehicles, IEEE Transactions on Power Electronics 27 (2012) 2752–2769.

[30] X. Hu, S. Li, H. Peng, A comparative study of equivalent circuit models for li-ion batteries, Journal of Power Sources 198 (2012) 359–367.

[31] O. Tremblay, L. A. Dessaint, Experimental validation of a battery dynamic model for EV applications, World Electric Vehicle Journal 3 (2009) 1–10.

[32] M. Ehsani, Y. Gao, A. Emadi, Modern electric, hybrid electric, and fuel cell vehicles: fundamentals, theory, and design, CRC press, 2010.

[33] J. Gao, F. Sun, H. He, G. Zhu, E. Strangas, A comparative study of supervisory control strategies for a series hybrid electric vehicle, in: Asia-Pacific Power and Energy Engineering Conference (APPEEC), 2009, pp. 1–7.

[34] T. Katrašnik, Analytical method to evaluate fuel consumption of hybrid electric vehicles at balanced energy content of the electric storage devices, Applied Energy 87 (2010) 3330–3339.

[35] A. Sciarretta, M. Back, L. Guzzella, Optimal control of parallel hybrid electric vehicles, IEEE Transactions on Control Systems Technology 12 (2004) 352–363.